High conversion efficiency of pristine TiO$_2$ nanotube arrays based dye-sensitized solar cells

WANG ShangHua[1,2], TAN WeiWei[1,2], ZHANG JingBo[1] & LIN Yuan[1*]

[1] *Beijing National Laboratory for Molecular Sciences, Key Laboratory of Photochemistry, Institute of Chemistry, Chinese Academy of Sciences, Beijing 100190, China;*
[2] *Graduate School of Chinese Academy of Sciences, Beijing 100049, China*

We prepared highly-ordered titanium dioxide nanotube arrays (TNAs) by anodizing Ti foils in F$^-$-containing electrolytes. The crystalline nature and morphology of the TNAs were studied using X-ray diffraction patterns and scanning electron microscopy. We found the morphology of TNAs affects the light-to-electricity conversion efficiency (η) of dye-sensitized solar cells (DSSCs). The efficiency of DSSCs reached 5.95% under the condition of light illuminated from the counter electrode. The high efficiency of TNA-based DSSCs was attributed to the neat top surface of TNAs, which allows more dye molecule loading on the surface of the TiO$_2$ nanotubes, and fewer electron recombination centers and a low interface resistance of integrated TNAs.

TiO$_2$ nanotube arrays, dye-sensitized solar cells, light-to-electricity conversion efficiency, photoanode, open-circuit voltage

Since the first paper by Regan and Grätzel [1], dye-sensitized solar cells (DSSCs) have been considered a relatively low-cost solar cell technology and potential alternative to silicon solar cells. As one of the main components of DSSCs, the properties of photoanodes have a great effect on the energy conversion efficiency of DSSCs. The efficiency of DSSCs is determined by the surface area of the photoanode, charge carrier transport in the semiconductor electrode, and electron recombination. In recent years, titanium dioxide nanotube arrays (TNAs) have received a great deal of attention, since Gong et al. [2] first reported their preparation in 2001. This is caused by the highly-ordered architecture of TNAs, which allows fast electron transport [3–5], and the structure, which influences the absorption and propagation of light [6]. However, the reported efficiencies of pristine TNA-based DSSCs are lower than the TiO$_2$ nanoparticle-based DSSCs when illuminated from the counter electrode [4,7–10]. Two factors decrease the efficiency of TNA-based DSSCs. The first is that the surface area of TNAs is

smaller than that of TiO$_2$ nanoparticles (TNP) [11]. Second, the counter electrode and the electrolyte absorb photons in the near-UV region when illuminated from the counter electrode [12,13]. To increase the surface area, TNAs can be treated with TiCl$_4$ [14–16], filled with nanotubes with TNP [17], or undergo an electrophoretic deposition of nanoparticles [11].

In this experiment, we prepared highly-ordered TNAs with a smooth top surface through the anodization of titanium foil in F$^-$-based electrolytes. The conversion efficiency reached 5.95%. We attributed the high efficiency to the smooth top surface, which made it easier for dye molecule loading on the wall of the nanotube; the fewer recombination centers in integrated TNAs; and the more efficient electron transport in highly-ordered TNAs.

1   Experimental

1.1   Materials

Lithium   iodide   (LiI),   4-tert-butylpyridine,   3-methoxyace-

*Corresponding author (email: linyuan@iccas.ac.cn)

tonitrile, 1-hexyl-2,3-dimethylimidazolium iodide, and iodine (I_2) were purchased from Acros Organics (Beijing). Ethylene glycol, acetone, methanol, ethanol, isopropanol, NH_4F, acetonitrile (CH_3CN), tetra-nbutyltitanate, butanol, acetic acid, and NaOH were purchased from Beijing Chemical Company (Analytic reagent grade). Ti foils were purchased from Alfa Aesar.

1.2   Preparation of photoanode and counter electrode

Pieces of Ti foil (99.5% purity, 1 cm×2 cm, 0.2 mm thickness) were used for the anodic growth of TNAs. They were sequentially polished with silicon carbide sandpaper of 400, 600, 800, 1000, and 1500 grit to obtain a mirror surface. After, they were ultrasonically cleaned in acetone, isopropanol, methanol, and deionized water for 10 min. They were dried under a stream of N_2 and used immediately.

The cleaned titanium foils were electrochemically anodized in a solution of 0.5 wt% NH_4F, 1 wt% deionized water, and 98.5 wt% ethylene glycol. The anodization was carried out in a two-electrode cell, using platinum foil as a counter electrode. Anodization was performed under constant voltage. The voltage was held at 60 V for 10–60 h. Subsequently, the prepared TNAs were washed with deionized water and dried in air. All the prepared TNAs were annealed at 500°C for 2 h and then cooled to room temperature. Then, the annealed TNAs were immersed in a 0.3 mmol/L ethanol solution of $Ru(dcbpy)_2(NCS)_2$ (N3, Solaronix) for 24 h.

Transparent Pt counter electrodes were prepared by spreading 5 mmol/L H_2PtCl_6 aqueous solution on an fluorine-doped SnO_2 transparent conductive glass (FTO) substrate, followed by heating at 390°C for 15 min.

1.3   Cell assembly and dye desorption

The dye-sensitized TNAs, the Pt-counter electrode, and the electrolyte solution, which was composed of 0.5 mol/L LiI, 0.05 mol/L I_2, and 0.5 mol/L 4-tert-butylpyridine in 3-methoxypropionitrile, were assembled into a sandwich cell structure. The dye desorption was carried out in 5 mL 0.01 mol/L NaOH to determine the dye loading amount on the surface of the nanotubes.

1.4   Characterization and instruments

The cells were illuminated with a Newport solar simulator (69911) under AM 1.5 (100 mW cm^{-2}) irradiation. Photoelectrochemical measurements were performed with a potentiostat/galvanostat (EG&G Princeton Applied Research, model 273) at room temperature. The morphologies of the TNA samples were observed using scanning electron microscopy (SEM, S-4300). X-ray diffraction (XRD) patterns were recorded with an X-ray diffraction meter (Rigaku D/max-2500, Cu Kα). Electrochemical impedance spectroscopy (EIS) data were obtained under 100 mW cm^{-2} il-

luminations, with a perturbation of ±10 mV over the open-circuit potential using a Solartron 1255B frequency analyzer and Solartron SI 1287 electrochemical interface system.

2   Results and discussion

2.1   Characterization of TNAs

Figure 1(a)–(c) show the top views of the TNAs anodized for 30, 50, and 60 h, respectively, showing that the TNAs are composed of highly-ordered vertically-oriented TiO_2 nanotubes. The inner diameter and the wall thickness of the nanotube are 90±5 and 20±2 nm, respectively. The smooth and orderly surface tubular structures of TNAs were gradually destroyed as the reaction time increased. As shown in Figure 1(a) and (b), the top surface of the nanotube is smooth and orderly. However, for the TNAs that were prepared for 60 h, some debris is present on the top surface of the nanotube arrays (Figure 1(c)). This debris is the dissolved part of the nanotube. Figure 1(c) shows that the mouth of the nanotube was destroyed and the top surface of the TNAs became rough and disordered. The cross- section images also show that the TNAs are composed of highly-ordered nanotubes (Figure 1(d)).

The anodization process contains two parts: electrochemical oxidation of titanium into amorphous TiO_2 and chemical dissolution of the oxide into soluble titanium fluoride species (TiF_6^{2-}). The electrochemical reaction and chemical reactions at the bottom and mouth of the nanotube are two main factors of the growth of TNAs. The formation of TNAs can be expressed by the competition between electrochemical oxidation (reaction 1) and chemical dissolution (reaction 2):

$$Ti + 2H_2O = TiO_2 + 4H^+ + 4e^- \qquad (1)$$

$$TiO_2 + 6F^- + 4H^+ = TiF_6^{2-} + 2H_2O \qquad (2)$$
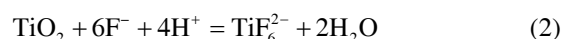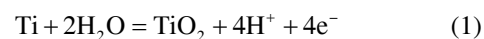
Metallic Ti is first oxidized to TiO_2 and then selectively dissolved by F^- ions. This makes the pore deeper. To produce a long nanotube, a proper acidic environment for the electrolyte must be controlled. In the high-viscosity electrolyte, the OH^- in the bulk solution and H^+ produced via reaction 1 have a lower diffusion rate. The pH value at the bottom of the tube is mainly controlled by reaction 1 and is much less influenced by the bulk electrolyte pH value. During the anodization process, the electrochemical oxide reaction rate at the bottom decreased gradually, but at the mouth the chemical dissolution reaction rate, which is mainly controlled by the bulk solution, remains unchanged. In the process of preparing TNAs, the thicknesses of TNAs first increase with time, but then stop increasing because the electrochemical reaction rate decreased as time increased. An overly long reaction time will destroy the highly-ordered architecture of TNAs.
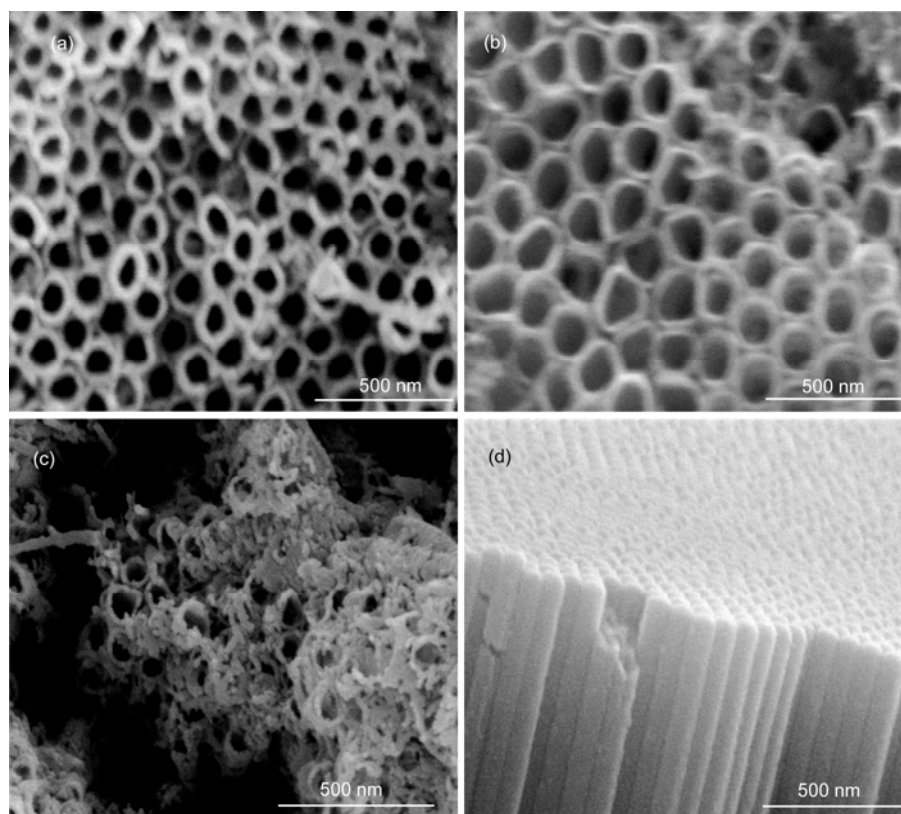
The dye loading amount is an important aspect of the

Figure 1   SEM images of the prepared TiO$_2$ nanotube arrays. (a) Top view of TNAs prepared for 30 h; (b) top view of TNAs prepared for 50 h; (c) top view of TNAs prepared for 60 h; (d) cross-section of TNAs prepared for 50 h.

light-to-electricity conversion efficiency of DSSCs. Longer nanotubes can provide a larger surface area for dye loading. The thickness of the TNAs prepared for 30, 50, and 60 h are 23, 35, and 33 μm, respectively. The more dye molecules loaded, the larger the short-circuit current density that will be obtained. In our work, TNAs were immersed in 0.3 mmol/L N3 ethanol solution overnight. After that, the wall of the TiO$_2$ nanotube was covered with a closely-packed mono-layer of N3 dye. The dye loading (d_l) amount can be determined from the equation:

$$d_l = \frac{AV}{\varepsilon S_0}, \tag{3}$$

where A, V, ε, and S_0 are the absorbance of the desorption solution, volume of desorption solution, molar extinction coefficient, and geometric area of the photoanode, respectively. The dye loading amounts are shown in Table 1. As shown in Table 1, the dye loading amount increased when the reaction time increased to 50 h. This occurs because longer nanotubes provide a larger surface area for dye load-ing. However, the dye loading amount did not increase when the reaction time was 60 h. This is because the rate of the electrochemical oxide reaction is slower than the chem-ical dissolution rate. Therefore, the length of the nanotube begins to decrease and the top of the nanotube had dissolved.

Table 1   Dye loading amount for the TNAs and photovoltaic performance parameters for the DSSCs

t (h)	d_l (10^{-7} mol cm^{-2})	J_{sc} (mA cm^{-2})	V_{oc} (mV)	ff	η (%)
30	0.94	7.57	742	0.75	4.24
50	1.44	10.35	748	0.77	5.95
60	1.34	11.25	692	0.70	5.46

2.2   XRD analysis

Figure 2 shows XRD patterns of the TiO$_2$ nanotube arrays before and after sintering. After sintering, the crystalline structure of the prepared TNAs changed from amorphous to polycrystalline anatase TiO$_2$ (identified by the (101) peak at $2\theta = 25.3°$) and the crystallite size was 20 nm. Other peaks corresponding to (200), (103), and (105) faces were also detected.

2.3   Photovoltaic performances

DSSC performance was measured with illumination from the counter electrode. The photovoltaic performance pa-rameters of the TNA-based DSSCs are shown in Figure 3 and the corresponding data are collected in Table 1. DSSCs based on TNAs prepared for 50 h have the highest η of
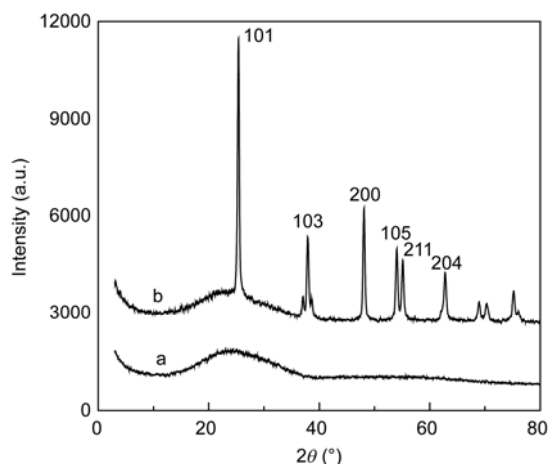
Figure 2 XRD patterns of the TiO$_2$ nanotube arrays before (a) and after (b) sintering.
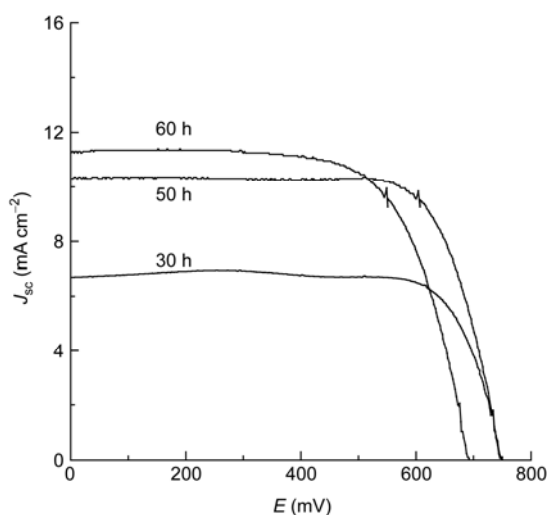

Figure 3 Current-voltage characteristics for the TNA-based DSSCs.

5.95%, while the 60 h TNA-based DSSCs have a lower open-circuit voltage (V_{oc}), fill factor (*ff*), higher short-circuit current density (J_{sc}), and lower η. The higher J_{sc} occurred because the barrier layer thickness between the nanotube and Ti substrate decreased, which is beneficial for the collection of photogenerated electrons. The destroyed TNAs and the debris provide more electron recombination centers for the electrons; therefore, the V_{oc} decreased. The lower fill factor probably occurs because the charge transport in the destroyed TNAs is not as efficient as that in integrated TNAs. For conversion efficiency, in the case of TNAs with similar thicknesses, the morphology is more important because the difference in the thickness is only 2 μm for TNAs prepared for 60 and 50 h.

2.4 EIS analysis

EIS is a powerful technique for studying porous electrodes.

EIS data were measured under 100 mW cm^{-2} illumination, using a perturbation of ±10 mV over the open-circuit potential. EIS plots are shown in Figure 4 and the corresponding impedance data are collected in Table 2. Two semicircles are present in the Nyquist plot. The semicircle at high frequency is attributed to the charge-transfer process occurring at the Pt counter electrode/electrolyte interface, and the semicircle at low frequency is attributed to the resistance at the photoanode/electrolyte interface. An equivalent circuit represented in Figure 4 (inset) was used for the fitting of impedance spectra for all cells with Zview software (Boukamp, UK). R_s, R_{ct}, and R_i describe series resistance, charge-transfer resistance, and resistance in the photoanode/electrolyte interface, respectively. R_s indicate that the reaction time has little effect on the series resistances. The slight differences in R_{ct} were ascribed to the different counter electrodes used in our experiments. The decrease in R_i is caused by increasing surface area. R_i began to increase when the reaction time was extended to 60 h. This occurred because the surface area of the destroyed TNAs is smaller than that of highly-ordered TNAs.

3 Conclusion

We prepared highly-ordered TNAs. The SEM images show that the TNAs have a highly-ordered architecture and the wall of the TiO$_2$ nanotubes is smooth. XRD data show that after sintering, the crystalline structure of the prepared TNAs changed from amorphous to polycrystalline anatase
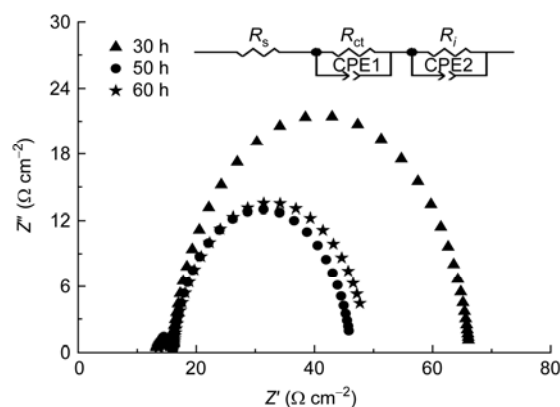

Figure 4 EIS plots of DSSCs based on TiO$_2$ nanotube arrays prepared using various reaction times.

Table 2 Parameters of electrochemical impedance spectroscopy obtained from Figure 4

t (h)	R_s (Ω)	R_{ct} (Ω)	R_i (Ω)
30	13.13	2.69	50.48
50	12.85	3.42	30.01
60	13.45	2.60	33.21

TiO$_2$. An overly long reaction time will destroy the highly-ordered TNAs and increase the R_i. The pristine TNA-based DSSCs have a higher efficiency of 5.95% when illuminated from the counter electrode. For conversion efficiency, in the case of TNAs with similar thicknesses, the morphology is more important. We attributed the high efficiency to the neat surface, which made it easier for dye molecule loading to occur on the wall of the nanotube. In addition, electron transport is more efficient in highly-ordered TNAs.

1   O'Regan B, Grätzel M. A low-cost, high-efficiency solar cell based on dye-sensitized colloidal TiO$_2$ films. Nature, 1991, 353: 737–740
2   Gong D, Grimes C A, Varghese O K, et al. Titanium oxide nanotube arrays prepared by anodic oxidation. J Mater Res, 2001, 16: 3331–3334
3   Frank A J, Kopidakis N, Lagemaat J. Electrons in nanostructured TiO$_2$ solar cells: Transport, recombination and photovoltaic properties. Chem Rev, 2004, 248: 1165–1179
4   Mor G K, Shankar K, Paulose M, et al. Use of highly-ordered TiO$_2$ nanotube arrays in dye-sensitized solar cells. Nano Lett, 2006, 6: 215–218
5   Kim D, Ghicov A, Albu S P, et al. Bamboo-type TiO$_2$ nanotubes: Improved conversion efficiency in dye-sensitized solar cells. J Am Chem Soc, 2008, 130: 16454–15455
6   Ong K G, Varghese O K, Mor G K, et al. Numerical simulation of light propagation through highly-ordered titania nanotube arrays: Dimension optimization for improved photoabsorption. J Nanosci Nanotechnol, 2005, 5: 1801–1808
7   Jennings J R, Ghicov A, Peter L M, et al. Dye-sensitized solar cells based on oriented TiO$_2$ nanotube arrays: Transport, trapping, and transfer of electrons. J Am Chem Soc, 2008, 130: 13364–13372
8   Stergiopoulos T, Ghicov A, Likodimos V, et al. Electrophoretic deposition of uniformly distributed TiO$_2$ nanoparticles using an anodic aluminum oxide template for efficient photolysis. Nanotechnology, 2008, 19: 235602
9   Yang D J, Park H, Cho S J, et al. TiO$_2$-nanotube-based dye-sensitized solar cells fabricated by an efficient anodic oxidation for high surface area. J Phys Chem Solids, 2008, 69: 1272–1275
10   Yang Y, Wang X H, Li L T. Synthesis and photovoltaic application of high aspect-ratio TiO$_2$ nanotube arrays by anodization. J Am Ceram Soc, 2008, 91: 3086–3089
11   Wang S H, Zhang J B, Chen S Y, et al. Conversion enhancement of flexible dye-sensitized solar cells based on TiO$_2$ nanotube arrays with TiO$_2$ nanoparticles by electrophoretic deposition. Electrochim Acta, 2011, 56: 6184–6188
12   Park J H, Lee T W, Kang M G. Growth, detachment and transfer of highly-ordered TiO$_2$ nanotube arrays: Use in dye-sensitized solar cells. Chem Commun, 2008, 25: 2867–2869
13   Ito S, Ha N L, Rothenberger G, et al. High-efficiency (7.2%) flexible dye-sensitized solar cells with Ti-metal substrate for nanocrystalline-TiO$_2$ photoanode. Chem Commun, 2006, 38: 4004–4006
14   Lei B X, Liao J Y, Zhang R, et al. Ordered crystalline TiO$_2$ nanotube arrays on transparent FTO glass for efficient dye-sensitized solar cells. J Phys Chem C, 2010, 114: 15228–15233
15   Li L L, Tsai C Y, Wu H P, et al. Fabrication of long TiO$_2$ nanotube arrays in a short time using a hybrid anodic method for highly efficient dye-sensitized solar cells. J Mater Chem, 2010, 20: 2753–2819
16   Lin C J, Yu W Y, Chien S H. Transparent electrodes of ordered opened-end TiO$_2$-nanotube arrays for highly efficient dye-sensitized solar cells. J Mater Chem, 2010, 20: 1073–1077
17   Chen J G, Chen C Y, Wu C G, et al. An efficient flexible dye-sensitized solar cell with a photoanode consisting of TiO$_2$ nanoparticle-filled and SrO-coated TiO$_2$ nanotube arrays. J Mater Chem, 2010, 20: 7201–7207